Optically generated small electron and hole polarons in nominally undoped and Fe-doped $KNbO_3$ investigated by transient absorption spectroscopy

S. Torbrügge, M. Imlau,* B. Schoke, C. Merschjann, and O. F. Schirmer
Fachbereich Physik, Universität Osnabrück, D-49069 Osnabrück, Germany

S. Vernay, A. Gross, V. Wesemann, and D. Rytz
FEE GmbH, D-55743 Idar-Oberstein, Germany

(Received 28 January 2008; revised manuscript received 20 May 2008; published 25 September 2008)

Transient light-induced absorption in nominally undoped and Fe-doped $KNbO_3$ crystals is observed in the visible and infrared spectral ranges after single pulse illumination with $\lambda=532$ nm. For nominally undoped $KNbO_3$ the decay of the light-induced absorption in a single step can be explained by incoherent hopping transport of optically generated small bound O^- hole and small free Nb^{4+} electron polarons and their mutual recombination. Iron doping causes an additional slow decay component and, remarkably, accelerates the initial decay process. A consistent model for the formation, hopping, and recombination paths of hole and electron polarons is deduced from the experimental data set for both nominally undoped and Fe-doped $KNbO_3$. The decrease in the polaron hopping-transport length in Fe-doped samples is attributed to the increased number densities of optically generated hole polarons by additional one-quantum excitations.

DOI: 10.1103/PhysRevB.78.125112 PACS number(s): 71.38.−k, 77.84.Dy

I. INTRODUCTION

Electrons in the conduction bands of most of the ABO_3 oxide perovskites tend to be self-trapped as small polarons (see, e.g., Refs. 1 and 2) at the B sites of the materials.[3] Corresponding hole polarons in the valence band are not known; however, such holes are rather trapped at deep acceptors, charged negatively with respect to the lattice. In this way the valence of, e.g., a transition-metal defect such as Fe^{3+} is increased to Fe^{4+}. In undoped material, however, acceptors are generally represented by cation vacancies; they are surrounded by several symmetry-equivalent O^{2-} ions. In such cases, the hole, bound to the acceptor, is usually self-trapped as a small polaron at one of these oxygen ions, being stabilized by lattice distortion.[4]

Contrary to charge-transport processes of tunneling free charge carriers, small polarons hop incoherently between the symmetry-equivalent sites;[1,2] free small polarons contribute in this way to the electrical dc conductivity. Independent of whether bound or free, small polarons are characterized by intense and wide optical-absorption bands, approximately having a Gaussian shape. This often causes the coloration of the materials.[1,2,4] Since such polarons can be created by optical excitations, they play an important role in optical damage processes in oxide nonlinear optical materials.[5] On the other hand, the analysis of light-induced formation and decay processes, monitored by the related optical absorptions, allows one to gain insight into the number densities of the metastably trapped carriers, the paths covered before recombination, the hopping of the free-electron polarons, and the detrapping of the bound hole polarons.[6] The lifetime of metastable small polarons depends, among others, on the hopping-transport length, the temperature, and the stabilization energy of the lattice deformation. Here, the hopping-transport length equals the sum of elementary hopping steps between neighboring B cation sites spanning the distance from creation to recombination. Doping with extrinsic defects allows for an intermediate trapping of quasifree charge carriers [e.g., at Fe^{2+}/Fe^{3+} sites in Fe-doped $LiNbO_3$ (Ref. 7)]. Hence, an influence of the doping on the intrinsic defect structure, and therefore on the hopping-transport length, can be expected as well.

This paper reports on the hopping-transport properties of metastable small polarons in potassium niobate ($KNbO_3$) crystals, i.e., of free Nb_{Nb}^{4+} electron polarons and of O^- hole polarons probably bound to potassium vacancies V_K. Both types of carriers are generated in nominally undoped and Fe-doped $KNbO_3$ crystals by intense nanosecond pulses of 532 nm light from a *Q*-switched frequency-doubled YAG:Nd laser. The pulse intensities are sufficient to produce valence-band holes and conduction-band electrons simultaneously by two-quantum transitions. In doped materials valence-band holes can also result from one-quantum excitations of valence-band electrons to Fe-related defects, having levels in the band gap of the material. The presence and decay of the electron and hole polarons is probed by the absorption of weak continuous-wave probe light at four wavelengths suited for the detection of the polaron and Fe-defect optical bands in $KNbO_3$. In nominally undoped $KNbO_3$, electrons and holes recombine in a single and fast decay process with a time dependence very well described by a stretched-exponential function. In contrast, in Fe-containing crystals a slowly decaying second stretched-exponential process is superimposed, and an acceleration of the fast process is found. The analysis of the data leads to a detailed understanding of the mechanisms governing the excitation, self-trapping, incoherent hopping, and recombination of the small polarons in $KNbO_3$. Also the influence of the Fe defects as intermediate trapping sites of hole polarons is clarified qualitatively. A possible contribution of Nb_{Nb}^{4+} and O^- polarons to the phenomenon of blue-light-induced infrared absorption (BLIIRA) in $KNbO_3$ (Ref. 8) can be suggested.

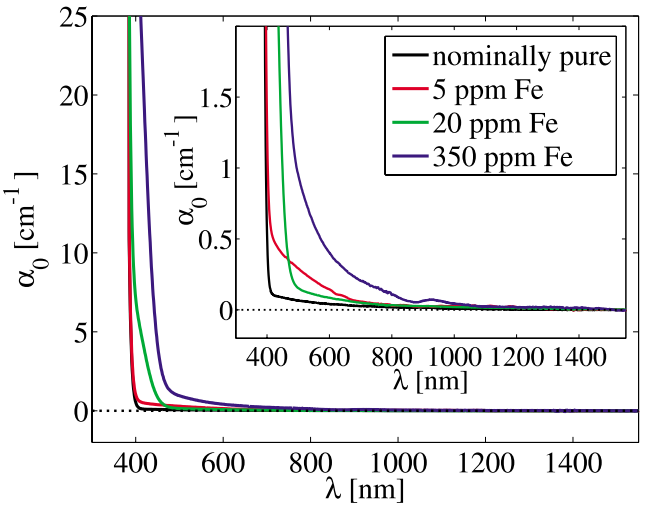

FIG. 1. (Color online) Optical steady-state absorption spectra (ordinary probe-light polarization) for nominally undoped and Fe-doped $KNbO_3$ single crystals. Doping concentrations: 5, 20, and 350 ppm Fe.

II. EXPERIMENTAL DETAILS AND RESULTS

Our investigations were performed with nominally undoped and Fe-doped $KNbO_3$ single crystals provided by FEE-Idar-Oberstein, Germany and the crystal-growth department of the University of Osnabrück, respectively. Samples of dimensions $a \times b \times c = 7 \times 3 \times 6$ mm^3 (nominally undoped) and $4 \times 3 \times 4$ mm^3 (Fe doped), respectively, were prepared from single-domain boules. The large a-c faces were polished to optical quality. The doping concentrations incorporated by adding Fe_2O_3 to the melt were 5, 20, and 350 ppm Fe in the crystals. Corresponding absorption spectra of the samples for ordinary probe light are shown in Fig. 1.

The spectra are corrected for reflection losses. The nominally undoped sample is highly transparent over the visible and near-infrared spectral ranges ($\alpha_0 < 0.1$ cm^{-1}). Its ultraviolet absorption edge[9] where the absorption coefficient equals 20 cm^{-1} lies at (385 ± 1) nm. Fe doping is reflected by a significant redshift of the band edge: (385 ± 1) nm for 5 ppm Fe, (387 ± 1) nm for 20 ppm Fe, and (419 ± 1) nm for 350 ppm Fe. This redshift is in accordance with findings in $LiNbO_3$, where the spectral position of the fundamental absorption edge is an indicator for the composition.[10] In comparison with nominally undoped $KNbO_3$, the absorption coefficient slightly increases in the visible and near-infrared spectral ranges by doping as depicted in the inset of Fig. 1. The sample with 350 ppm Fe exhibits a weak absorption band at 925 nm of unknown origin.

The samples were investigated by pump-probe-laser spectroscopy [cf. inset of Fig. 2(a)] using single intense laser pulses of a Q-switched frequency-doubled YAG:Nd laser for pumping ($\lambda_{pump} = 532$ nm, $\tau_{FWHM} = 8$ ns, and maximum pulse intensity $I_{pump} = 705$ GW/m^2). During and after the pulse, the transmitted intensities $I_{probe}(t)$ of four discrete probe-laser beams are monitored simultaneously ($\lambda_{probe} = 488$, 633, 785, and 1310 nm and $I \leq 1.6$ kW/m^2). Intensities were detected by appropriate PIN diodes. The signals

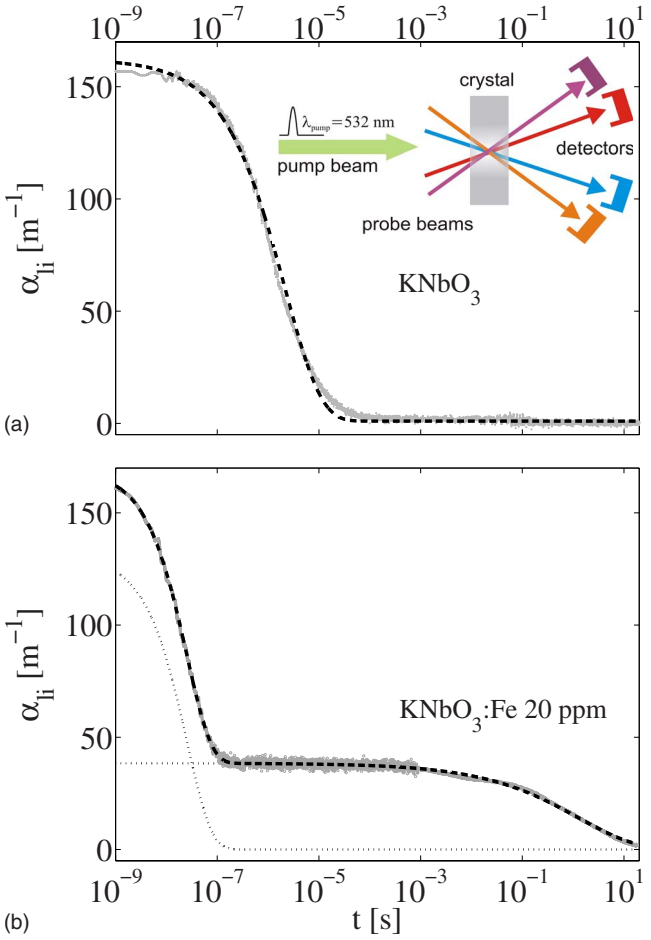

FIG. 2. (Color online) Temporal evolution of $\alpha_{li}(t)$ at $I_{pump} = 420$ GW/m^2 and $\lambda_{probe} = 785$ nm for (a) undoped $KNbO_3$ and (b) 20 ppm Fe-doped $KNbO_3$. The dashed lines represent fits according to Eq. (2) with parameters (a) $\alpha_{li}^{fast} = (162 \pm 10)$ m^{-1}, $\tau^{fast} = (2.1 \pm 0.8)$ μs, and $\beta^{fast} = (0.61 \pm 0.05)$, respectively. (b) Fast component: $\alpha_{li}^{fast} = (130 \pm 5)$ m^{-1}, $\tau^{fast} = (0.03 \pm 0.01)$ μs, and $\beta^{fast} = (0.91 \pm 0.10)$; and slow component: $\alpha_{li}^{slow} = (38 \pm 5)$ m^{-1}, $\tau^{slow} = (1.3 \pm 0.2)$ s, and $\beta^{slow} = (0.38 \pm 0.05)$ (dotted lines). The inset in (a) sketches the pump-probe geometry of our experimental setup.

from the detectors are amplified and fed into a digital storage oscilloscope. If not indicated otherwise, all measurements were carried out at room temperature. Ordinary pump and probe-light polarizations were chosen to get the maximum signal amplitude (cf. Refs. 7 and 11). From $I_{probe}(t)$ the temporal behavior of the light-induced absorption $\alpha_{li}(t)$ was determined by

$$\alpha_{li}(t) = \frac{1}{d} \ln \left[\frac{I_{probe}(t \leq 0)}{I_{probe}(t)} \right], \tag{1}$$

with the effective crystal thickness d.

Figure 2 shows the characteristic temporal evolutions of the light-induced absorption $\alpha_{li}(t)$ for (a) a nominally undoped and (b) an Fe-doped $KNbO_3$ sample (20 ppm Fe), respectively.

Note that a logarithmic time scale is chosen. The pump intensity was $I_{pump} = 420$ GW/m^2 and the data were shown

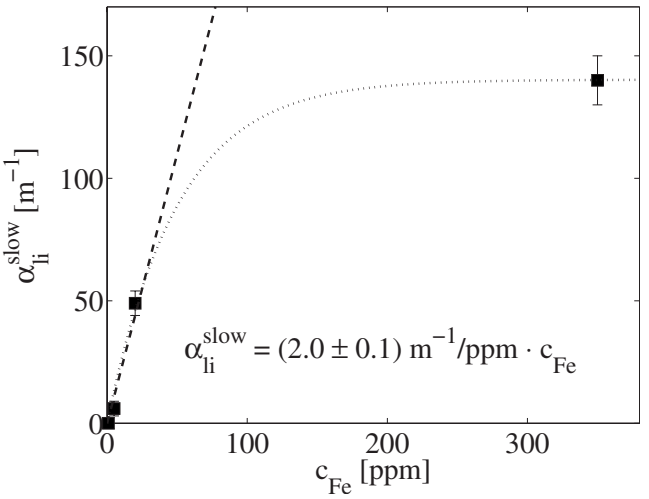

FIG. 3. Amplitude α_{li}^{slow} of the slow decay component as a function of iron concentration ($I_{pump}=705$ GW/m^2 and $\lambda_{probe}=785$ nm). The dashed line represents a linear fit to the experimental data set. The dotted line is a guide to the eyes.

as an example for a probe wavelength of $\lambda_{probe}=785$ nm. A light-induced absorption with comparable maximum value of $\alpha_{li}^{max}=155$ and 160 m^{-1}, respectively, appeared immediately after the pump pulse in the two samples. Obviously, the buildup of $\alpha_{li}(t)$ could not be resolved with our setup and is to be expected in the range below 1 ns (cf. Ref. 12). After the pump pulse, the light-induced absorption shows a temporal decrease to zero. Remarkably, there are fundamental differences in the relaxation kinetics of the two samples: For the nominally undoped sample, α_{li} relaxes from its maximum value in a single step to zero and, hence, vanishes already completely after about 100 μs. In contrast, for the Fe-doped sample, the relaxation process has to be divided into two decay components in analogy to the results of Buse and Krätzig.[11] The first decay relaxes within 0.1 μs from its maximum value to $\approx$40 m^{-1} and vanishes to zero in a second step within about 10 s.

The temporal behavior of the decays can be modeled neither by a single-fold nor by a twofold exponential function. For decay processes related to polaronic charge transport, the relaxation is best described by a stretched-exponential function of type $\alpha_{li}(t)=\alpha_{li,0}\exp[-(t/\tau)^{\beta}]$ (see, e.g., Refs. 13 and 14). Here, $\alpha_{li,0}$, τ, and β are the maximum amplitude, the characteristic time constant, and the stretching factor of the decay component, respectively. A single stretched-exponential function is fitted to the relaxation kinetics of $\alpha_{li}(t)$ of the nominally undoped sample. The fit is represented in Fig. 2(a) by the dashed line and yields the fit parameters as given in the figure caption. In contrast, a sum of two stretched-exponential functions, one for the fast and one for the slow decay component, was fitted to the Fe-doped $KNbO_3$ sample according to

$$\alpha_{li}(t) = \alpha_{li}^{fast}\exp[-(t/\tau^{fast})^{\beta^{fast}}] + \alpha_{li}^{slow}\exp[-(t/\tau^{slow})^{\beta^{slow}}]. \quad (2)$$

The least-squares fit to the measured data is represented by the dashed line in Fig. 2(b). Note that the fast and slow decay components of the fit are plotted separately as dotted lines.

TABLE I. Parameters determined from fitting Eq. (2) to the experimental data $\alpha_{li}(t)$ of nominally undoped and Fe-doped samples at maximum pump-beam intensity of $I_{pump}=705$ GW/m^2 and for the probe wavelength $\lambda_{probe}=785$ nm.

c_{Fe}[ppm]	<1	5	20	350
α_{li}^{fast}[m^{-1}]	(305 ± 20)	(193 ± 10)	(177 ± 10)	(14 ± 5)
τ^{fast}[μs]	(2.0 ± 0.8)	(0.6 ± 0.3)	(0.03 ± 0.01)	(0.01 ± 0.01)
β^{fast}	(0.56 ± 0.10)	(0.69 ± 0.10)	(0.89 ± 0.15)	(0.49 ± 0.10)
α_{li}^{slow}[m^{-1}]		(6 ± 3)	(49 ± 5)	(140 ± 10)
τ^{slow}[ms]		(12 ± 3)	(435 ± 35)	(1120 ± 85)
β^{slow}		(0.14 ± 0.05)	(0.38 ± 0.05)	(0.39 ± 0.05)

The two-step relaxation process of stretched-exponential type was observed in the $KNbO_3$ samples doped with 5 and 350 ppm Fe at the probe wavelength of 785 nm, as well. Exemplarily, the related fit parameters determined at maximum pump-beam intensity ($I_{pump}=705$ GW/m^2) are given in Table I.

Remarkably, we found that the lifetime of the fast decay component τ^{fast} decreases and the amplitude α_{li}^{slow} increases with higher doping concentration. This dependence suggests that the fast decay component τ^{fast} found in the Fe-doped samples may have the same origin as the single decay component of the nominally undoped sample. At the same time, the second decay component α_{li}^{slow} has to be assigned to the presence of Fe.

From the plot $\alpha_{li}^{slow}(c_{Fe})$ shown in Fig. 3 we notice a linear increase in α_{li}^{slow} particularly for small Fe concentrations. Fitting a linear function to the data set yields $\alpha_{li}^{slow}(c_{Fe})=[(2.0\pm0.1)\ \text{m}^{-1}/\text{ppm}]c_{Fe}$. This might be applied as a tool for the determination of residual Fe impurities in $KNbO_3$ crystals.

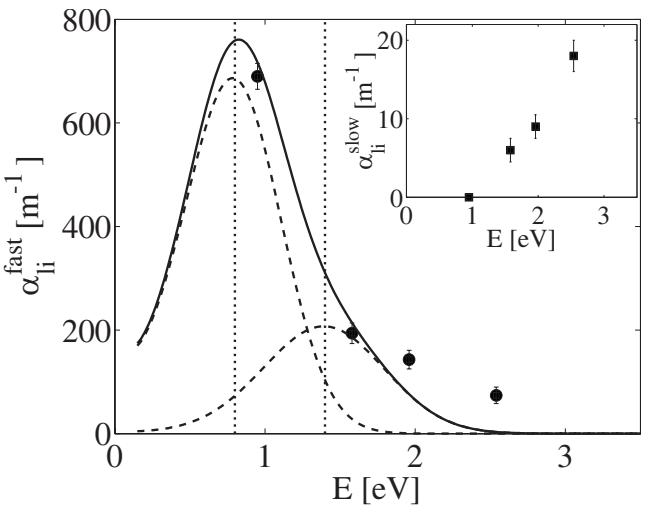

FIG. 4. Dispersion of the maximum amplitudes α_{li}^{fast} and α_{li}^{slow} (see inset) related to the photon energy E of the probe beam for $KNbO_3$:Fe (5 ppm) ($I_{pump}=705$ GW/m^2). The solid line represents a superposition of two small polaron bands (individually indicated by the dashed lines) peaking at 0.8 and 1.4 eV, respectively, and adjusted in their amplitudes to reproduce the experimental data.

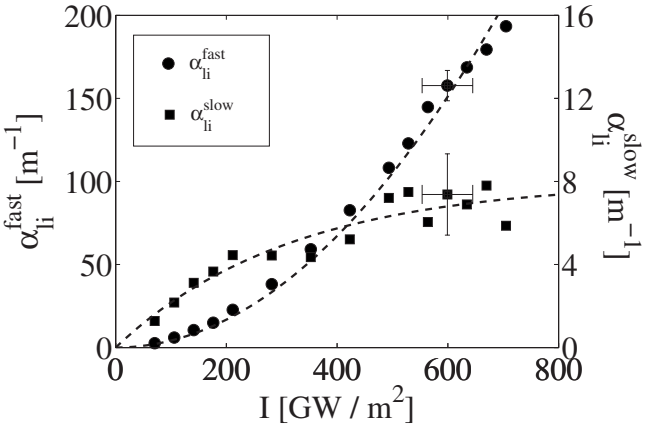

FIG. 5. Dependence of α_{li}^{fast} and α_{li}^{slow} on the pump-beam intensity for the $KNbO_3$ sample doped with 5 ppm Fe (λ_{probe} =785 nm). Dashed lines indicate fits to the experimental data with a quadratic function and according to Eq. (3), respectively. Fit parameters: $K=(4.2\pm0.5)\times10^{-4}$ m^3/GW^2 for the fast decay and $\alpha_{li,sat}^{slow}=(8\pm2)$ m^{-1} and $I_{pump}^{sat}=(317\pm20)$ GW/m^2 for the slow decay.

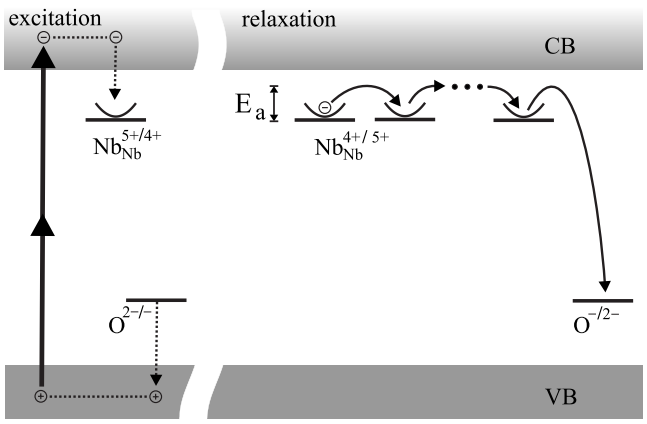

FIG. 6. Schematic description for the different mechanisms of excitation (left side) and relaxation of small polarons via hopping (right side) in nominally undoped $KNbO_3$. Thick solid arrows denote excitation by pump light and dotted arrows mean trapping of electrons/holes on polaron levels. Note that the energy levels are shown only schematically; they do not represent absolute defect energies.

The dispersion of the maximum amplitudes $\alpha_{li}^{fast}(\lambda_{probe})$ and $\alpha_{li}^{slow}(\lambda_{probe})$ with respect to the probe beam wavelength yields the spectra shown in Fig. 4.

The values are given as an example for the $KNbO_3$ sample doped with 5 ppm Fe and result from the two-component fitting procedure. The data set is plotted as a function of the photon energy of the probe beam. Obviously, the amplitudes of the fast and slow decays obey a complementary behavior. While α_{li}^{fast} decreases with increasing photon energy from 690 m^{-1} at 0.95 eV ($\simeq$1310 nm) to 74 m^{-1} at 2.54 eV ($\simeq$488 nm), α_{li}^{slow} increases with increasing photon energy (see inset of Fig. 4). Comparable results for the fast decay component were obtained for all samples including the nominally undoped one. However, we note that at 1310 nm the amplitude of the fast component is remarkably twice as high for the 5 ppm Fe-doped sample in comparison with the nominally undoped sample. In contrast, we could not resolve the slow decay component at this wavelength.

Figure 4 additionally shows the plotted shapes of two individual small polaron bands[2,4] (dotted lines) proportional to $(1/E)\exp[-(2E_p-E)^2/(4E_p\hbar\omega_0)]$. Here, E is the photon energy, E_p is the polaron stabilization energy, and $\hbar\omega_0$ is the longitudinal optical phonon energy. According to Sec. III A, the photon energies 0.8 and 1.4 eV as well as $E_p(Nb^{4+})$ =0.45 eV and $E_p(O^-)$=0.75 eV (Refs. 4, 15, and 16) have been applied. For $\hbar\omega_0$ the value of 0.1 eV was assumed, typical for polarons in oxide materials.[4] The solid line represents the superposition of the two individual small polaron bands. Only the relative amplitudes of both component bands in Fig. 4 were adjusted.

The kinetics of the light-induced absorption were investigated as a function of temperature from 25 °C up to 65 °C limited by the formation of randomly aligned domains at higher temperatures. The lifetimes of all decay components in all samples obey an Arrhenius law according to $\tau(T)=(1/Z)\exp[E_a/(k_BT)]$. Here, Z is the frequency factor, E_a is the thermal activation energy, k_B is the Boltzmann constant, and T is the absolute temperature of the crystal. The fits yield an activation energy $E_a^{fast}=(0.14\pm0.05)$ eV for the fast decay component independent of the probe wavelength and doping concentration. The activation energy of the slow decay component strongly varies as a function of the probe wavelength: (0.38 ± 0.06) eV at 488 nm, (0.61 ± 0.07) eV at 633 nm, and (0.82 ± 0.09) eV at 785 nm. The obtained maximum amplitudes as well as the stretching factors for both decays did not reveal a temperature dependence.

Finally, the dependence of the maximum amplitudes of fast and slow decay components was investigated as a function of pump-beam intensity. As an example, Fig. 5 displays the dependencies $\alpha_{li}^{fast}(I_{pump})$ and $\alpha_{li}^{slow}(I_{pump})$ for the $KNbO_3$ sample doped with 5 ppm Fe.

A quadratic increase in $\alpha_{li}^{fast}(I_{pump})$ is obvious and can be fitted by $\alpha_{li}^{fast}(I_{pump})=KI_{pump}^2$. In contrast $\alpha_{li}^{slow}(I_{pump})$ saturates at high pump-beam intensities according to

$$\alpha_{li}^{slow}(I_{pump}) = \alpha_{li,sat}^{slow}\left[1-\exp\left(-\frac{I_{pump}}{I_{pump}^{sat}}\right)\right], \qquad (3)$$

where $\alpha_{li,sat}^{slow}$ denotes the saturation value of the slow decay component of the light-induced absorption and I_{pump}^{sat} is the characteristic intensity. The quadratic dependence of the maximum amplitude α_{li}^{fast} on the pump-beam intensity is found for the nominally undoped $KNbO_3$ sample, as well. This underlines again that the fast decay component in the doped samples can be identified with the single decay component in the nominally undoped sample.

III. DISCUSSION

Our systematic study on the light-induced absorption upon nanosecond-pulse exposure in nominally undoped and Fe-doped $KNbO_3$ samples obviously reveals two key results with respect to the contribution of Fe to the recombination

behavior: The Fe doping (1) accelerates the dominating fast decay component and (2) it induces the appearance of a second slow decay component of the light-induced absorption. The found stretched-exponential behavior of both decay components with characteristic lifetime and stretching factor is a typical property of polaronic charge-transport processes and can be attributed to a hopping-like charge transport via polaronic levels.[17,18] Equivalent stretched-exponential relaxations therefore are observed in various oxide crystals with rich intrinsic and extrinsic defect structures investigated with pump-multiprobe-laser spectroscopy.[7,13,14,19,20]

Taking into account previous results of electron-paramagnetic resonance (EPR) investigations[21,22] and the results of radiation-induced absorption,[15,23,24] we can discuss our findings in the frame of the intrinsic and extrinsic defect structure of $KNbO_3$ and, in particular, in the frame of excitation and recombination processes of small electron and hole polarons. We take advantage of the fact that the structure of $KNbO_3$, including the possible defect structures, can be considered as closely related to $BaTiO_3$ and $KTaO_3$.

A. Intrinsic origin of the fast decay component

The results show that the presence of the Fe dopant is not required for the appearance of the fast decay component of the relaxation process. We hence can conclude that this decay has to be accomplished with the intrinsic defect structure of $KNbO_3$. Here, Nb_{Nb}^{4+} free-electron polarons and O^- bound hole polarons with absorption maxima at about 0.8 eV (Ref. 15) and at about 1.4 eV,[16] respectively, have to be considered. We would like to note that the experimentally determined value of 1.4 eV is close to the theoretically predicted one, 1.1 eV.[23] The hole polaron is trapped most likely near a potassium vacancy V_K (Refs. 23 and 25) and behaves thus like a small bound polaron. Only a hole polaron bound to such a K-site acceptor will cause an absorption band peaked below 1.5 eV.[4] Since free O^- hole polarons are unlikely to occur in oxide ABO_3 perovskites, in the following, we will mean by hole polarons bound ones.

The first decay component features a quadratic dependence of its maximum amplitude α_{li}^{fast} on the pump-beam intensity. This points to a two-photon process for excitation. Taking into account the band gap of $KNbO_3$ of approximately 3.3 eV,[21] which fairly well corresponds to the position of the band gap found in the absorption spectra in Fig. 1, we can assume creation of free charge carriers by band-to-band excitation.

This will simultaneously result in an electron self-trapping at Nb_{Nb}^{5+}, forming small Nb_{Nb}^{4+} polarons, and in hole capture near a potassium vacancy yielding small bound O^- polarons[4,23,24] as schematically depicted in Fig. 6 (left side).

In this case, the light-induced absorption, particularly at $\lambda = 1310$ and 785 nm in Fig. 4, originates from the superposition of the electron and hole-polaronic absorption bands. For this reason, the individual shapes of the small Nb_{Nb}^{4+} polaron and of the small bound O^- polaron peaking at 0.8 and 1.4 eV have been added[2,4] in Fig. 4. Obviously, their superposition expected on this basis reasonably reproduces the experimental data (solid lines in Fig. 4). With respect to the slight discrepancies at the higher energies, it can be remarked that the given theoretical band shapes tend to underestimate the experimental polaron absorptions in the energy range above their peak energies.[4]

As a consequence of this model the relaxation of the fast decay component resembles the recombination of free Nb_{Nb}^{4+} electron and O^- hole polarons by hopping charge transport via Nb_{Nb} polaron levels (right side in Fig. 6). This is particularly supported by the determined activation energy $E_a \approx 0.14$ eV (cf. Figure 6), which is close to that expected from the peak energy $E_m \sim 0.8$ eV (Ref. 23) of the related optical-absorption band (Refs. 1 and 2) $E_a \sim 1/4 E_m$. In comparison with the theoretically deduced activation energy for O^- of ≈ 0.5 eV (Ref. 25) it is apparent that the charge transport in the excited state is dominated by electron migration via the Nb_{Nb} centers.

B. Acceleration of the fast decay component by Fe doping

The lifetime of the light-induced absorption depends on the effective polaron hopping-transport length until recombination occurs. We remind that the hopping-transport length equals the sum of elementary hopping steps between neighboring B cation sites spanning the distance from creation to recombination. Obviously, the lifetime can be decreased if the number density of recombination partners or the polaron mobility is increased. Applied to $KNbO_3$:Fe, the lifetime of the electron-polaron to hole-polaron recombination process depends on the charge transport in the free Nb_{Nb}^{4+} polaron level as well as on the number density of the O^- hole polarons or, possibly, of additional other recombination partners, i.e., extrinsic defect centers having captured a hole. Since the experimentally determined activation energy of the fast decay showed no dependence on the doping concentration, we conclude that charge-transport processes via the Nb_{Nb}^{4+} polaron level are not influenced by Fe doping. Hence, an increased number density of deep traps due to an increased number of O^- hole polarons or due to additional extrinsic defects has to be assumed to explain the accelerated decay of the fast component within this model. The first case is supported by the increased light-induced absorption in $KNbO_3$:Fe in the infrared spectral range where hole polarons have their absorption maximum. But also the presence of Fe is clearly observed in the light-induced absorption spectra of $KNbO_3$:Fe, reflecting the slow decay process. The increase in the O^- hole-polaron number density can be explained within the model in Fig. 7 taking into account the Fe doping via the additional X center. Details of the relation between the X center and the Fe doping are discussed in Sec. III C.

In analogy to the model for the nominally undoped $KNbO_3$ (Fig. 6) Nb_{Nb}^{4+} electron and O^- hole-polaron centers are populated by two-quantum excitations also for Fe-doped material. This is well supported by our experimental findings for the fast decay (activation energy independent on Fe doping, quadratic dependence on the pump-beam intensity, etc.). In contrast to the nominally undoped sample, the presence of the X center in principle allows optical excitations of electrons from X^0 to the conduction band or from the valence

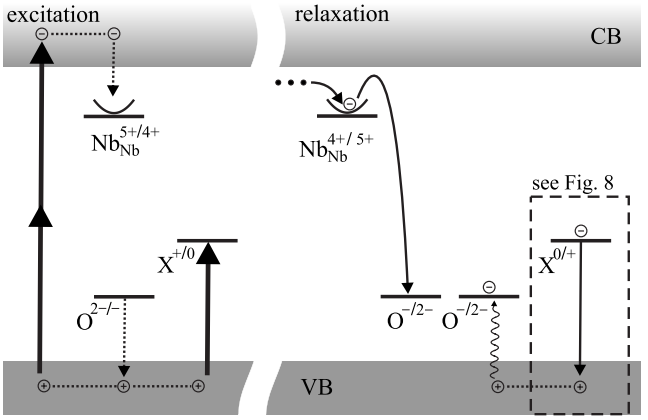

FIG. 7. Mechanisms for the excitation (left side) and relaxation (right side) in $KNbO_3$ doped with iron. In addition to the two-quantum excitation from the valence band (VB) to the conduction band (CB), an excitation of electrons from the VB into an X center leads to an increased density of holes and, hence, of hole polarons. Thick solid arrows: excitation by pump light; dotted arrows: trapping of electrons/holes on polaron levels; and wavy solid arrows: thermal excitation.

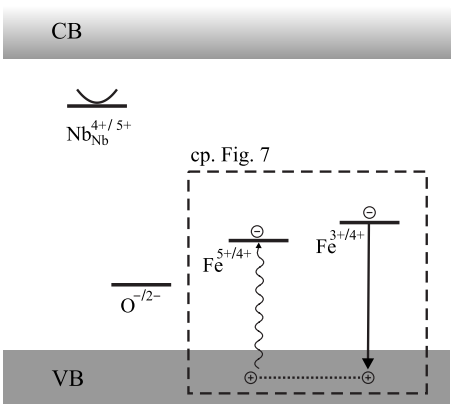

FIG. 8. More detailed scheme for the processes related to the X center in Fig. 7 in analogy to the model presented in Ref. 22.

band to X^+, respectively. Transitions from cation defects to the conduction band, having mainly Nb character, are *next*-nearest-neighbor transitions. Hence, they are comparatively weak unless the related cation defect level is close to the conduction band, equivalent to a large extension of the wave function of the defect. Transitions from the valence band, mainly having oxygen character, are always nearest-neighbor transitions and thus relatively strong. Hence, and according to the findings in related materials such as $BaTiO_3$,[22] the second type of one-photon processes will dominate. This will be accompanied by the formation of holes in the valence band, which are expected to be trapped subsequently as bound hole polarons. The creation of additional O^- hole polarons as recombination partners will thus depend on the number density of X levels and will be the natural consequence of Fe doping. We therefore can conclude that the lifetime of the fast decay process should decrease with increasing number density of X centers, i.e., with the increasing Fe concentration. This model is clearly consistent with the results presented in Table I. The number of free-electron polarons is determined by the band-to-band two-quantum excitations independent of the presence of Fe defects. Therefore, additional O^- holes, which have been created by one-quantum transitions to the X centers, will be left over after polaronic electron-hole recombination. While present, they increase the probability of recombination with the electrons. Those holes not consumed in this process will again be trapped at the X level. This intermediate storage of the holes is responsible for the second slow decay component of the light-induced absorption.

We would like to note that our study in $KNbO_3$:Fe remarkably uncovers an entirely different behavior of the transient absorption than in Fe-doped $LiNbO_3$.[7] The initial value of the light-induced absorption in $LiNbO_3$ first increases, reaches its maximum value at approximately 10^{-4} s, and finally shows a single relaxation process when probing Fe-doped samples with light in the blue-green spectral range (Fig. 2 in Ref. 7). We can attribute this remarkable difference to the following two facts: (1) The energetic positions of the absorption bands of the Fe^{2+} center and O^- hole polaron are both centered in the blue-green spectral range near 2.5 eV in $LiNbO_3$. In $KNbO_3$, the O^- hole polaron is centered at 1.4 eV. The differences in the O^- peak positions result from the fact that in $LiNbO_3$ the V_{Li} binding defect is surrounded by six nearly equivalent oxygen sites, whereas V_K in $KNbO_3$ has twelve equivalent oxygen neighbors.[4] (2) In $LiNbO_3$ the electron-hole-polaron recombination is decelerated by charge trapping of the electrons at the Fe center as an intermediate step. In contrast, holes are captured at the Fe center in $KNbO_3$, i.e., the Nb_{Nb}^{4+}-O^- recombination path remains unaffected.

C. Nature of the X center

We will now discuss the possible nature of the X center taking into account our experimental findings related to the second slow decay component (dispersion of activation energy and of maximum amplitudes of the light-induced absorption). Obviously, from Fig. 7, it follows that optical excitations of electrons from the valence band to the X center are accompanied by strong charge-transfer absorption bands. Such processes are typically observed for cation defects with higher valence states in oxide perovskites. Because these X-related phenomena are seen to increase with Fe doping, it is likely that Fe is involved in the structure of the X defects. Numerous Fe-containing defects in Fe-doped $KNbO_3$ have been identified previously,[16,22] but detailed information on their structure could not yet be obtained. Hence, the presumed defect scenario will be discussed on the basis of available knowledge in the related perovskite oxides $KTaO_3$ and $BaTiO_3$. A summary on such defects can be inferred from the Appendix.

The band scheme depicted in Fig. 8 allows one to explain the slow recombination process in $KNbO_3$:Fe. One-quantum transitions of the type shown have been established repeatedly for $BaTiO_3$:Fe.[22,28] After two-quantum optical excitation of the crystal, the available valence-band holes will partly be trapped also at the shallower levels, i.e., at $Fe^{5+/4+}$.

TABLE II. Fe-containing defects in Fe-doped $KTaO_3$, $BaTiO_3$, and $KNbO_3$ with positions of the absorption bands in eV, where available.

$KTaO_3$ (Refs. 22 and 27)		$BaTiO_3$ (Ref. 22)		$KNbO_3$ (Refs. 16 and 22)
Fe_{Ta}^{3+}	(3.5 eV)	Fe_{Ti}^{2+}	(2.1 eV)	Fe_{Nb}^{3+}
Fe_{Ta}^{3+}-V_O	(3.3 eV)	Fe_{Ti}^{3+}	(>3 eV)	Fe_{Nb}^{3+}-V_O
Fe_{Ta}^{3+}-?	(3.2 eV)	Fe_{Ti}^{4+}	(2.7 eV)	Fe_{Nb}^{3+}-X
Fe_{Ta}^{3+}-Fe_K^{3+}		Fe_{Ti}^{5+}	(2.3 eV)	Fe_{Nb}^{3+}-Y
Fe_{Ta}^{2+}	(1.5 eV)	Fe_{Ti}^{3+}-V_O		Fe_{Nb}^{3+}-Z
Fe_{Ta}^{2+}-V_O	(1.5 eV); (2.8 eV)	Fe_{Ti}^{4+}-V_O		$Fe_{?}^{3+}$
Fe_K^{4+}-O_I	(1.8 eV); (2.8 eV)			Fe_K^{+}
Fe_K^{3+}				
Fe_K^{+}				

This hole capture is connected with a light-induced absorption change α_{li} with respect to the equilibrium situation, where holes can exist at most at the deeper level ($Fe^{4+/3+}$). Thermal excitation of valence-band electrons to the shallower $Fe^{4+/5+}$ levels and the subsequent recombination of the created valence-band holes with electrons from the deeper one, $Fe^{3+/4+}$, will restore the initial absorptive state of the crystal leading to $\alpha_{li}=0$. We note that this model is only a minimal one since various other Fe defects in $KNbO_3$ can lead to further related gap levels. Nevertheless, it successfully serves to explain the presented data set. Equivalent considerations were necessary to explain the photorefractive properties in Fe-doped $KNbO_3$.[29]

D. Blue-light-induced infrared absorption

Our results may give a hint in identifying shallow and deep traps involved in the phenomenon of BLIIRA.[8] The intrinsic nature of the shallow trap was already suggested by Buse and Krätzig.[11] Here, it turns out that Nb_{Nb}^{4+} electron and O^- hole polarons could essentially participate in BLIIRA because of their pronounced light-induced absorption in the infrared spectral range. In contrast, although long living, the contribution of the slow component to the blue-light-induced absorption might be less significant because BLIIRA in Fe-doped samples is not much different from nominally undoped crystals.[8]

IV. CONCLUSION

Concluding our results, the light-induced absorption with a fast decay behavior can be related to the formation and recombination of Nb_{Nb}^{4+} electron polarons with O^- hole polarons. Its shorter lifetime in Fe-doped samples is a result of an increased number density of O^- hole polarons upon optical pumping. The larger amount of hole polarons results from the additional optical transfer of electrons to an (extrinsic) trap center via one-quantum excitation. The second slow decay process of the light-induced absorption can be related unambiguously to the presence of Fe in the $KNbO_3$ samples. Unfortunately, a clear assignment of the additional trap center to Fe, and particularly to its valence states, cannot be deduced from our investigations. Which of the conceivable valence states of Fe (2+/3+/4+/5+) are present in $KNbO_3$ hence remains an open question. Furthermore, it cannot be excluded that in addition to such isolated defects also associations of Fe with other lattice perturbations, such as oxygen vacancies, are involved in the process.

In the frame of analytical spectroscopy, these results allow nevertheless to determine the content of Fe impurities in $KNbO_3$ samples by contact-free pump-probe-laser spectroscopy. In particular it is shown that samples of high purity (<1 ppm) are characterized by a single decay of the light-induced absorption and a lifetime of 2 μs.

ACKNOWLEDGMENTS

The financial support from the Deutsche Forschungsgemeinschaft (Project Nos. TFB 13-04 and IM 37/5-1) is gratefully acknowledged.

APPENDIX

Table II gives an overview on Fe-containing defects in $KNbO_3$, $KTaO_3$, and $BaTiO_3$. Most of the entries have been assigned by studies of EPR, optically detected paramagnetic resonance, and combined EPR-optical studies. The lower valencies are usually found in reduced material; the higher ones in as-grown or oxidized crystals. In $BaTiO_3$, Fe_{Ti}^{2+} causes intervalence transitions from the defect to the conduction band,[26] whereas charge-transfer transitions occur from the valence band to Fe_{Ti}^{4+} and Fe_{Ti}^{5+}. The shown defects define a series of levels in the band gap of the materials, from which optical and/or thermal charge exchange of charge carriers with the conduction and valence bands can occur. Defects with higher valencies tend to have levels in the lower half of the gap and are likely to lead to thermal and optical excitations of holes to the valence band.

*mimlau@uos.de

[1] I. G. Austin and N. F. Mott, Adv. Phys. **18**, 41 (1969).
[2] D. Emin, Phys. Rev. B **48**, 13691 (1993).
[3] S. Lenjer, O. F. Schirmer, H. Hesse, and T. W. Kool, Phys. Rev. B **66**, 165106 (2002).
[4] O. F. Schirmer, J. Phys.: Condens. Matter **18**, R667 (2006).
[5] L. E. Halliburton, N. C. Giles, and Th. H. Myers, West Virginia University Research Corporation Final Technical Report No. A342373, 2003 (unpublished).
[6] M. Imlau, Phys. Status Solidi A **204**, 642 (2007).
[7] P. Herth, T. Granzow, D. Schaniel, T. Woike, M. Imlau, and E. Krätzig, Phys. Rev. Lett. **95**, 067404 (2005).
[8] H. Mabuchi, E. S. Polzik, and H. J. Kimble, J. Opt. Soc. Am. B **11**, 2023 (1994).
[9] I. Földvári, K. Polgár, R. Voszka, and R. N. Balasanyan, Cryst. Res. Technol. **19**, 1659 (1984).
[10] L. Kovács, G. Ruschhaupt, K. Polgár, G. Corradi, and M. Wöhlecke, Appl. Phys. Lett. **70**, 2801 (1997).
[11] K. Buse and E. Krätzig, Opt. Mater. **1**, 165 (1992).
[12] O. Beyer, D. Maxein, T. Woike, and K. Buse, Appl. Phys. B: Lasers Opt. **83**, 527 (2006).
[13] D. Berben, K. Buse, S. Wevering, P. Herth, M. Imlau, and T. Woike, J. Appl. Phys. **87**, 1034 (2000).
[14] S. Wevering, J. Imbrock, and E. Krätzig, J. Opt. Soc. Am. B **18**, 472 (2001).
[15] Y. Qiu, K. B. Ucer, R. T. Williams, L. Grigorjeva, D. Millers, and V. Pankratov, Nucl. Instrum. Methods Phys. Res. B **191**, 98 (2002).
[16] A. Mazur, Ph.D. thesis, Osnabrück University, 1999.
[17] B. Sturman, E. Podivilov, and M. Gorkunov, Phys. Rev. Lett. **91**, 176602 (2003).
[18] J. Carnicero, M. Carrascosa, G. García, and F. Agulló-López, Phys. Rev. B **72**, 245108 (2005).
[19] C. Merschjann, D. Berben, M. Imlau, and M. Wöhlecke, Phys. Rev. Lett. **96**, 186404 (2006).
[20] P. Herth, D. Schaniel, T. Woike, T. Granzow, M. Imlau, and E. Krätzig, Phys. Rev. B **71**, 125128 (2005).
[21] M. Zgonik, M. Ewart, C. Medrano, and P. Günter, in *Photorefractive Materials and Their Applications 2*, Springer Series in Optical Sciences, Vol. 114, edited by P. Günter and J.-P. Huignard (Springer, New York, 2007), Chap. 7, pp. 205–240.
[22] B. Briat, V. G. Grachev, G. I. Malovichko, O. F. Schirmer, and M. Wöhlecke, in *Photorefractive Materials and Their Applications 2*, Springer Series in Optical Sciences Vol. 114, edited by P. Günter and J.-P. Huignard (Springer, New York, 2007), Chap. 2, pp. 9–49.
[23] L. Grigorjeva, D. K. Millers, V. Pankratov, R. T. Williams, R. I. Eglitis, E. A. Kotomin, and G. Borstel, Solid State Commun. **129**, 691 (2004).
[24] L. Grigorjeva, Solid State Commun. **104**, 327 (1997).
[25] E. A. Kotomin, R. I. Eglitis, A. V. Postnikov, G. Borstel, and N. E. Christensen, Phys. Rev. B **60**, 1 (1999).
[26] A. Mazur, O. F. Schirmer, and S. Mendricks, Appl. Phys. Lett. **70**, 2395 (1997).
[27] N. Hausfeld, Ph.D. thesis, University of Osnabrück, 1999.
[28] E. Possenriede, P. Jacobs, H. Kröse, and O. F. Schirmer, J. Phys.: Condens. Matter **4**, 4719 (1992).
[29] K. Buse and E. Krätzig, Appl. Phys. B: Lasers Opt. **61**, 27 (1995).